Experimental Study of Natural Convection from an Array of Square Fins

Article *in* Experimental Thermal and Fluid Science (EXP THERM FLUID SCI) · January 2018

DOI: 10.1016/j.expthermflusci.2018.01.020

3 authors, including:

Amirreza Keyhani
Georgia Institute of Technology
8 PUBLICATIONS **20** CITATIONS

SEE PROFILE

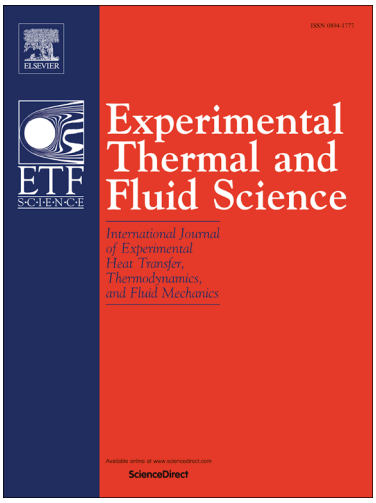

Experimental Study of Natural Convection from an Array of Square Fins

Mehdi Karami, Mahmood Yaghoubi, Amirreza Keyhani

PII: S0894-1777(18)30047-5
DOI: https://doi.org/10.1016/j.expthermflusci.2018.01.020
Reference: ETF 9343

To appear in: *Experimental Thermal and Fluid Science*

Received Date: 2 December 2017
Revised Date: 7 January 2018
Accepted Date: 14 January 2018

Please cite this article as: M. Karami, M. Yaghoubi, A. Keyhani, Experimental Study of Natural Convection from an Array of Square Fins, *Experimental Thermal and Fluid Science* (2018), doi: https://doi.org/10.1016/j.expthermflusci.2018.01.020

Experimental Study of Natural Convection from an Array of Square Fins

Mehdi Karami[a], Mahmood Yaghoubi[a,b,*], Amirreza Keyhani[c]

[a)]*School of Mechanical Engineering, Shiraz University, Shiraz, 71936-16548, Iran*
[b)]*The Academy of science of IR Iran, P.O. Box 19735/167, Tehran, Iran*
[c)]*The George W. Woodruff School of Mechanical Engineering, Georgia Institute of Technology, Atlanta, GA 30332-0405, USA*

*Corresponding author at: School of Mechanical Engineering, Shiraz University, Shiraz 71348-51154, Iran

Email address: mkarami@shirazu.ac.ir (M. Karami), yaghoubi@shirazu.ac.ir (M. Yaghoubi), akeyhani3@gatech.edu (A. Keyhani).

Abstract

In this research, we experimentally investigate natural convection heat transfer of three finned-tube exchangers with an array of square fins and a fin spacing of 5, 9, and 14 mm. The exchangers are in a $5.8\text{m}\times4\text{m}\times3\text{m}$ control room where temperature and humidity are automatically controlled with heating, cooling, humidifying, and dehumidifying equipment. We changed the surface temperature of the center tube by varying the input power of the heating element from 8.4 to 56.7 Watts. To measure the temperature of various points on each exchanger, we used ten T-type thermocouples and conduct four experiments for each exchanger and measured its temperature under the steady-state condition. We also calculated average natural heat transfer coefficient. The results show that amount of radiation heat transfer to the surroundings is about 10%, and the contribution of natural convection is approximately 80% of the total input power to the heating element for all experiments. In addition, average natural heat transfer coefficient increases to a certain value and then decreases when fin spacing increases. Finally, from the results of experiments, we established an empirical relationship in an equation for predicting Nusselt number when the Rayleigh number is between 6.5 and 1,335, based on the fin spacing.

Keywords: Natural convection, Finned tube, Nusselt number, Square fin, Heat transfer coefficient

Nomenclature

A	surface area $\left(\text{m}^2\right)$
d	tube diameter $\left(\text{mm}\right)$
F	view factor
g	acceleration of gravity $\left(\text{m.s}^{-2}\right)$
k	thermal conductivity $\left(\text{W.m}^{-2}.\text{K}^{-1}\right)$
k_a	thermal conductivity of air
s	fin spacing $\left(\text{mm}\right)$
n	number of fins

t time (min)

T temperature $(^{\circ}\text{C})$

Q_{Total} total heat transfer rate (W)

Q_{Conv} convection heat transfer rate (W)

Q_{Rad} radiation heat transfer rate (W)

Q_{Loss} heat loss from the insulation surface (W)

Q_{Cond} conduction heat transfer (W)

r equivalent radius of the fin (mm)

ΔT temperature difference, $T_s - T_a$

$\bar{h}$ average convection heat transfer coefficient $(\text{W.m}^{-2}.\text{K}^{-1})$

$\overline{Nu_s}$ average Nusselt number, $\bar{h}\, s/k_a$

Nu_s Nusselt number, $h\, s/k$

L fin height (mm)

Ra_s^* Rayleigh number, $\dfrac{g\,\beta(T_s - T_a)s^3}{\alpha\,\nu}\left(\dfrac{s}{L}\right)$

T_f film temperature, $\dfrac{T_s + T_a}{2}$

RH relative humidity $(\%)$

Subscripts

a ambient air

i inner

o outer

s surface

al aluminum

Greek Symbols

α thermal diffusivity $(\text{m}^2.\text{s}^{-1})$

β volumetric thermal expansion coefficient $\left(\mathrm{K}^{-1}\right)$

δ fin thickness $\left(\mathrm{mm}\right)$

ε emissivity

ν kinematic viscosity $\left(\mathrm{m}^2.\mathrm{s}^{-1}\right)$

σ Stephan-Boltzmann constant, $5.67\times10^{-8}\,\mathrm{W.m^{-2}.K^{-4}}$

ε_f Fin effectiveness

1. Introduction

The subject of heat dissipation occupies a central place in the design of various engineering systems such as electronic cooling, solar collectors, and nuclear reactors involved in the thermal transport phenomenon. Two widely used thermal transport mechanisms for removing generated heat from systems are free and force convection. In both approaches, a reliable method of enhancing convection heat transfer is to use extended surfaces or fins. As a result, fins are widely used in many applications such as heating, ventilation, and air conditioning systems (HVAC), finned-tube heat exchangers, solar systems, electronic cooling, and electrical systems. The wide range of applications has spawned a large number of studies using analytical, computational, and experimental approaches to exploring natural convection heat transfer from finned surfaces.

In an early experimental study, Elenbaas [1] investigated natural convection heat transfer from two parallel plates with a gap of *s*. He showed that dissipated heat to the ambient environment is a function of *s* the temperature of the plates. He also introduced a new parameter for the correlation of natural convection heat transfer from parallel plates with a gap of *s* and a height of *H*, $Ra_s^* = Ra_s\left(s/H\right)$. Later, Sparrow and Bahrami [2] used naphthalene sublimation technique for experimental determination of natural convection heat flux on the faces of isothermal annular fins fixed to a heated, horizontal tube. Following similar experimental approaches, Edwards and Chaddock [3], Knudsen and Pan [4], and Jones [5] determined natural convection heat transfer from tubes with circular fins. These studies covered various scenarios from the geometry of tubes and fins to material composition, resulting in some correlations for prediction of heat transfer from circular fins.

Kayansayan and Karabacak [6] experimentally investigated natural convection heat transfer from a horizontal isothermal tube with circular fins vertically attached to the tube. They carried out experiments over 16 test cases and changed the controlling parameters such as fin spacing (s), temperature difference between the surfaces of the central tube and ambient temperature, ratio of outer diameter of the tube to the inner diameter (D/d), and ratio of the fin diameter to the tube diameter. They also analyzed heat dissipated by radiation from the assembly to the ambient environment. This study provides an empirical correlation over the range of controlling parameters. In another experimental study, Hahne and Zhu [7] used a thermo-visual method to obtain temperature distribution and mean heat transfer coefficient of a finned tube. They varied fin diameter for three test cases to find the effect of fin height on heat transfer. Their results revealed that for identical conditions, sets of shorter fins are more efficient than taller fins for heat dissipation. In an analytical and experimental study, Wang et al. [8] developed a comprehensive model for predicting natural convection heat transfer from annular vertical isothermal fins fixed to the central tube. This study revealed that heat dissipated from the end surfaces and fin rims has a significant effect on total heat transfer. Their correlation agrees with the results of previous studies.

In the recent literature, Yildiz and Yüncü [9] experimentally investigated natural convection heat transfer for annular fin arrays vertically on a horizontal cylinder by changing the fin diameter, fin spacing, and the base-to-ambient temperature difference. This study showed that all these three parameters determine convection heat transfer rate. In addition, for any fin diameter and for a given base-to-ambient temperature difference, there is an optimum value of fin spacing in which the heat transfer rate is maximum. In another recent study, Chen et al. [10, 11] found average natural convection heat transfer coefficient and fin efficiency of vertical square and annular fins on circular finned-tube heat exchangers. This study used finite difference and least-squares methods as well as experimentally measured temperature for specific cases. The results reveal a non-uniform temperature distribution across the fin surface and show that heat transfer coefficient in the lower regions of the fins is significantly higher than that in the upper regions. In addition, this study used an inverse method to find average heat transfer coefficient, which does not require solving the governing differential equations of the air flow near the fins. Furthermore, several other studies used extended surfaces with various shapes such as vertical

cylinders with plate fins [12-15] and various heat transfer phenomena such as frost formation on a finned-tube heat exchanger [16] and natural dehumidification over an annular finned tube [17].

Unlike finned tubes with annular fins, tubes with square fines have not been sufficiently studied. However, tubes with square fins are widely used in various devices such as economizers in coal- and oil-fired units or waste incinerators and air coolers. To provide practical insights, we experimentally investigate natural convection heat transfer from an array of square fins vertically attached to a horizontal tube. For the experiments, we designed and manufactured three finned tubes with different fin spacing. During the experiments, we preserved ambient temperature and humidity and change the base-to-ambient temperature difference. This study provides a new correlation based on experimental data to determine the Nusselt number as a function of Rayleigh number.

2. Experimental layout

2.1. Test room

For the experiments, we use a control room similar to that used in [16-18]. Figure 1 illustrates a schematic diagram of the test room. The used equipment consists of a cooling unit, a heating unit, a humidifier unit, an air temperature, humidity sensor, and measurement system, wall and ceiling temperature measurement probes, a test case, a data logger for the recording of the test case temperatures and humidity, and a thermograph Testo-881 system. The room dimension is sufficiently large for the test case dimensions, $5.8\mathrm{m}\times4\mathrm{m}\times3\mathrm{m}$. The air temperature, relative humidity, and test case temperature are adjustable. The test room is divided into two separate sections. The section on the left, the equipment section, contains the cooling unit, the heating unit, and the humidifier. The one on the right (i.e., the test section) contains the test case, cameras, and temperature and humidity measurement sensors. Dimensions of the test section are $4\mathrm{m}\times3\mathrm{m}\times4\mathrm{m}$. The two sections are separated by an insulated wall and partially connected by a channel embedded in the ceiling and the wall, shown in Fig. 1.

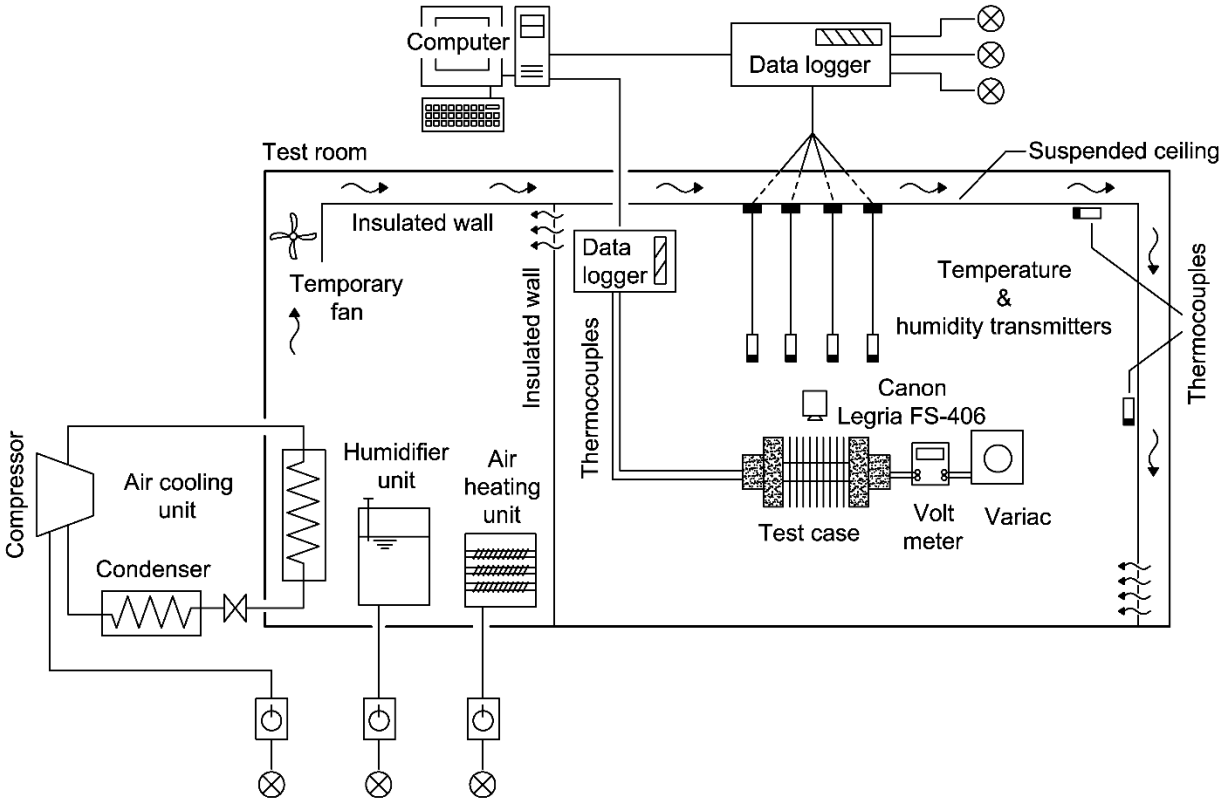

Fig. 1. Schematic diagram of the test room

During the experiment, the cooling, heating, and humidifier units adjust the temperature and the humidity of the equipment section, and this adjusted air flows to the test section through the fan and the channel. For a decreased and uniform air velocity in the test section, a diffused gate and a netted plate are embedded at the inlet and the end of the channel, respectively. At the netted plate, the airflow velocity is slightly less than 0.4 m/s. Since the test case is far from the entrance of the airflow in the test room (i.e., netted plate), the airflow does not affect natural convection of the test case and the units run for short periods. The cooling unit consists of four main parts: the compressor, the condenser, the expansion valve, and the evaporator. The compressor and the condenser are outside of the test room, and the evaporator is in the equipment section. The compressor power is 1.12 KW. The cooling unit can decrease temperature of the test room to 18°C. The heating unit consists of three thermal elements with a total power of 2 KW, which can increase the temperature of the test room to 50°C. The humidifier system uses two reservoirs with a total capacity of 12 liters. With 1.5 KW power, this

system preserves as much as 70% humidity for 12 hours in the test room. Cooling, heating, and humidifier units are automatically controlled with respect to the point datasets.

2.2. Temperature and humidity measurement system

We developed a system that continuously measures temperature and humidity of the test room and compares the measured values to the point dataset and then runs cooling, heating, and humidifier systems accordingly. This system includes three main parts: (1) temperature and relative humidity sensors, (2) data logger, and (3) controlling software (i.e., Look-Out). To simultaneously measure the temperature and the humidity of the test room, we used four TMH-1 type sensors and transmitters. This system has the capability of measuring temperatures between -40°C and +123.8°C with an accuracy of ±0.4°C and a range in the relative humidity of 0-100% with an accuracy of ±1%. Although the sensors are pre-calibrated in the factory, we also calibrate them for each test case. Data from measurements is transferred to a computer for processing by a data acquisition system (MOXA-ioLogik-E2210). Then, the Lookout program, which compares data with a point dataset adjusted by a user, manages the cooling, heating, and humidifier units accordingly. Furthermore, to analyze radiation heat transfer between the test case and the walls and ceiling, we used three sensors with an accuracy of ±0.3°C to measure their relative temperatures.

2.3. Test cases

In this study, we build three finned-tube exchangers from aluminum alloy with thermal conductivity of 177 $W.m^{-2}.K^{-1}$, shown in Figs. 2(a)-2(c). The dimensions of the fins are equal for all test cases. To eliminate contact resistance between the fins and the inner tube, we build each exchanger from a single block of aluminum. The length of each exchanger is 200 mm, and the length of the covered zone with fins is 100±1 mm. At both sides of each unit, a length of 50 mm with no fin is extended for the supporting frame and insulation. The inner and outer diameters of all tubes are 24 mm and 28 mm, respectively. The square fins are $100\,\text{mm} \times 100\,\text{mm}$ and 2 mm thick, and the fin spacing for the three exchangers are 5, 9, and 14 mm, respectively. To prevent heat loss from the outer surfaces of the terminal fins on both sides, the test sections

are insulated with glass wool covered by a layer of aluminum foil, shown in Figs. 2(d)-2(f). The geometrical parameters of the three test cases are listed in Table 1.

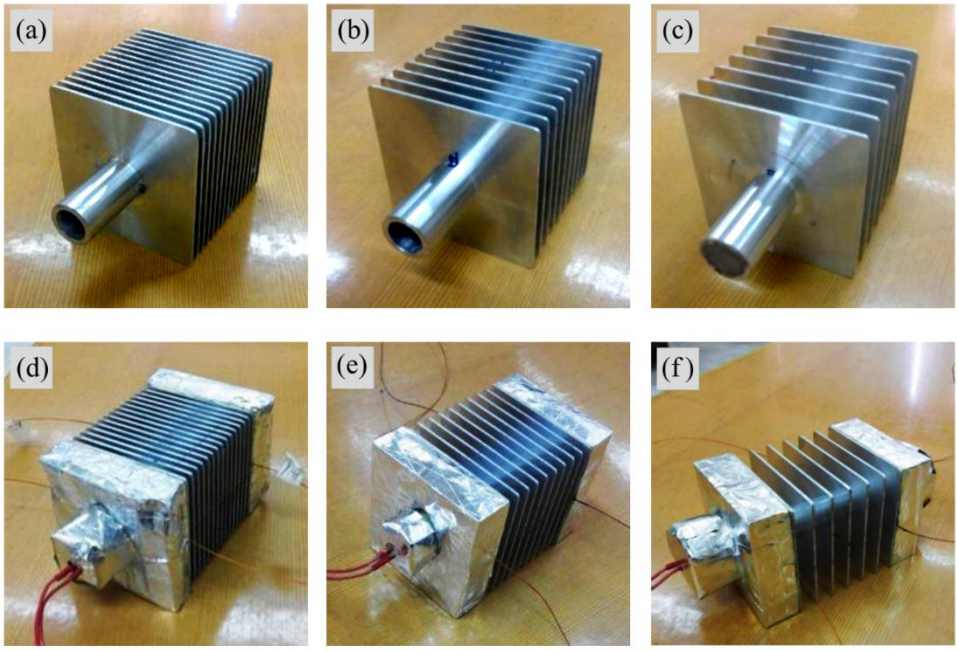

Fig. 2. Test cases: (a) *s*= 5 mm, (b) *s*=9 mm, and (c) *s*=14 mm. Test cases with end insulation: (d) *s*=5 mm, (e) *s*=9 mm, and (f) *s*=14 mm

Table 1. Geometrical features of the finned-tube exchangers.

Inner diameter of the tube (mm)	Outer diameter of the tube (mm)	Fin dimensions (mm×mm)	Fin spacing (mm)	Fin thickness (mm)	Number of fins (n)
24	28	100×100	5	2	15
24	28	100×100	9	2	10
24	28	100×100	14	2	7

2.4. Test-case temperature measurement and recording system

We used a system that continuously measures and records temperatures of a test case. Accordingly, this system controls and adjusts the fin base temperature. This system provides input for computation of heat transfer rate from the test case to its surroundings. Based on the temperature range for the tests, we use T-type thermocouples (copper/constantan) with a cross-section diameter of 1.1 mm with an accuracy of ±0.5°C. During the experiments, the data

acquisition unit (ADAM4518) transfers the measured temperature values to a computer. To measure the insulated surface temperature, we use a single-channel thermometer Testo 925 with a K-type sensor and a surface probe. This thermometer can measure temperatures in a range of 50°C to 1,000°C with an accuracy of ±0.5°C. To increase temperature of the tube, we used a 350-watt heating element connected to a variac transformer responsible for producing variable heat flux in the central tube and fin bases. To measure power consumed by the heating element, which is equal to thermal power in the test case, we used a Yaxun DT-9205A+ multimeter with ±0.01A accuracy. Figure 3 illustrates the experimental setup and the configuration of equipment in the control room.

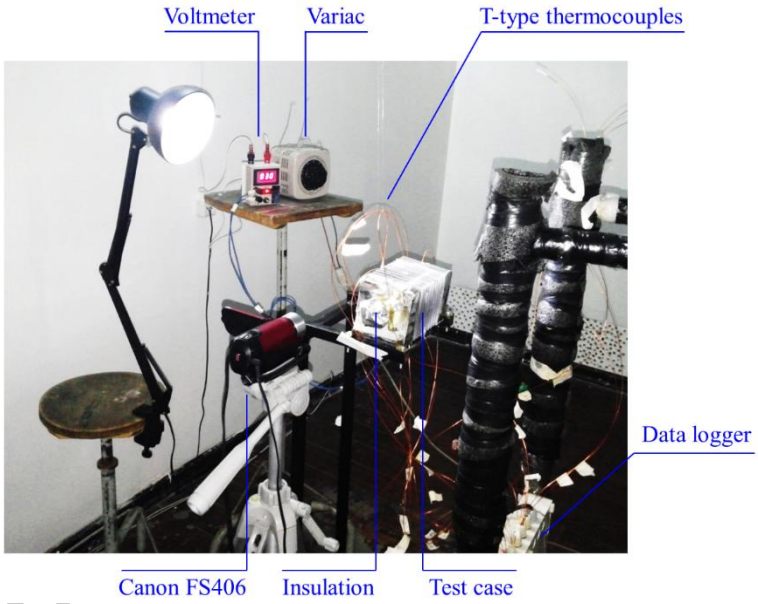

Fig. 3. Experimental setup with a test case on the support

In this study, we used three types of the temperature sensors: (1) the test room air temperature and humidity measurement sensors, (2) the test room wall and ceiling temperature measurement sensors, and (3) the test case temperature measurement thermocouples. To calibrate the test room air temperature and humidity measurement sensors, we used a mini-temperature and humidity data logger (Testo174H), which simultaneously measures temperature and the humidity of the test room with an accuracy of ±0.1°C and ±1%, respectively. For the calibration process of these sensors, we varied the room temperature between 20°C to 50°C and

collected data from the sensors. Then, we compared these data with the Testo174H measurements and calibrated the sensor measurements in Lookout software by inserting a third-order polynomial equation for the temperature and a second-order polynomial for the humidity. To ensure the accuracy of measurements, we followed a similar procedure for other sensors and performed the calibration process multiple times.

3. Results and Discussion

The following sections present results of the twelve series of experiments, which we designed and performed to determine convection heat transfer coefficient. The test conditions are listed in Table 2.

Table 2. Experimental conditions of all tests

Test No.	Fin spacing, s (mm)	Potential difference, ΔV	Current, I (A)	Heat Flux (W)	Room Temperature (°C±0.4)	RH (%±1.0)
1	5	30	0.29	8.7	23	40
2	5	50	0.38	19.0	23	40
3	5	70	0.48	33.6	23	40
4	5	90	0.60	54.0	23	40
5	9	30	0.28	8.4	23	40
6	9	50	0.38	19.0	23	40
7	9	70	0.48	33.6	23	40
8	9	90	0.62	55.8	23	40
9	14	30	0.28	8.4	23	40
10	14	50	0.37	18.5	23	40
11	14	70	0.49	34.3	23	40
12	14	90	0.63	56.7	23	40

3.1. Repeatability

We used the temperatures of the central tube surface (T1) and the fin rim (T10) as characteristic parameters and recorded variations in these parameters versus time for multiple experiments to evaluate the repeatability of the experiments. Figure 4 illustrates the temperature variations of T1 and T10 versus time for two experiments with an input power of 55.5 watts. Specifically, Fig. 4(a) compares the results of the two experiments under the steady-state condition for a fin spacing of 5 mm while Figs. 4(b) and 4(c) compare the results of the two tests

under transient and steady-state conditions for the fin spacing's of 9 mm and 14 mm, respectively. The result of the two tests are in good agreement for all cases, confirming repeatability of the experiments.

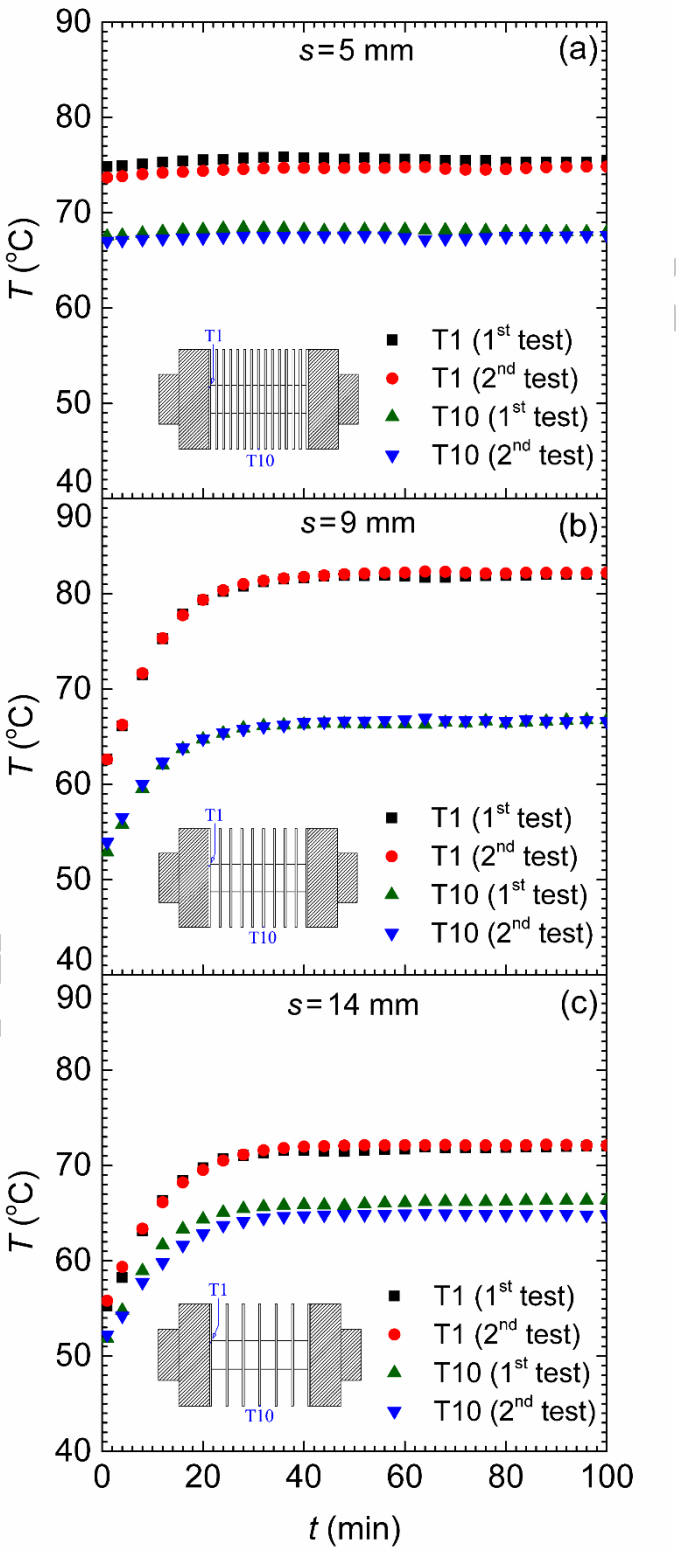

Fig. 4. Temperature variations of the reference points versus time for repeatability test

3.2 Radiation heat transfer from the test cases

Generated heat in the test cases resulting from conversion of electrical power to heat in the heating element transfers to the test case surroundings in three ways: (1) radiation heat transfer from the test case surface to the ambient environment, (2) convection heat transfer, and (3) heat loss from end insulation, all of which are described by the following equation:

$$Q_{Total} = Q_{Cond} = Q_{Conv} + Q_{Rad} + Q_{Loss}, \tag{1}$$

which are heat generated by the heating element, transferred heat from the heating element to the test case by conduction, heat transfer caused by convection, heat transfer caused by radiation, and heat loss from end insulation, respectively.

Estimation of transferred heat caused by radiation and heat loss from the end surfaces is necessary for calculation of convection heat transfer coefficient. To find the amount of transferred heat by radiation, this study uses the following equation [19]:

$$Q_{rad_{1-2}} = \frac{\sigma\left(T_1^4 - T_2^4\right)}{\frac{1-\varepsilon_1}{\varepsilon_1 A_1} + \frac{1}{A_1 F_{1-2}} + \frac{1-\varepsilon_2}{\varepsilon_2 A_2}}, \tag{2}$$

where $Q_{rad_{1-2}}$ is the radiation heat rate from surface 1 to surface 2 and σ is the Stephan-Boltzmann constant $\left(\sigma = 5.67\times10^{-8}\ \mathrm{W/m^2.K^4}\right)$; T_1, T_2, ε_1, ε_2, A_1, A_2, and F_{1-2} are the absolute temperature of surface 1, the absolute temperature of surface 2, the emissivity of surface 1, the emissivity of surface 2, the area of surface 1 (m^2), the area of surface 2 (m^2), and the view factor of body 1 to body 2, respectively. We use the method proposed by Hirbodi and Yaghoubi [17] to find the view factor of the finned-tube surface with respect to its surroundings. In previous studies, the shapes of fins were annular, but in our study, the fins are square. The equivalent radius of an square fin $\left(r_{eq}\right)$ with width w_{fin} and height h_{fin} [20] follows:

$$r_{eq} = \sqrt{\frac{w_{fin} \times h_{fin}}{\pi}}\ . \tag{3}$$

Based on Eq. (2), total radiation from n fins can be as follows:

$$Q_{rad} = (n-1)Q_{rad,i} + nQ_{rad,o_f}, \tag{4}$$

$$Q_{rad,i} = \frac{\sigma\left(T_i^4 - T_a^4\right)}{\frac{1-\varepsilon_i}{\varepsilon_i A_i} + \frac{1}{A_i F_{i-a}} + \frac{1-\varepsilon_a}{\varepsilon_a A_a}}, \tag{5}$$

$$Q_{rad,o_f} = \frac{\sigma\left(T_o^4 - T_a^4\right)}{\frac{1-\varepsilon_o}{\varepsilon_o A_{o_f}} + \frac{1}{A_{o_f} F_{o-a}} + \frac{1-\varepsilon_a}{\varepsilon_s A_a}}. \tag{6}$$

Here, $Q_{rad,i}$ and Q_{rad,o_f} represent radiation heat transfer delivered to the surroundings from the inner and outer surfaces of a finned tube, respectively; ε_i and ε_o are the emissivities of the inner and outer surfaces, which are equal to 0.09; coefficient F_{o-a}, the view factor of fin rims to its surroundings, is equal to 1; T_i, T_o, and T_a are the lateral and inner surface temperature of the fin, the surface temperature of the fin rim, and the ambient temperature, respectively. We used ten thermocouples to find temperature of the fin rim and the finned-tube surface, shown in Fig. 5.

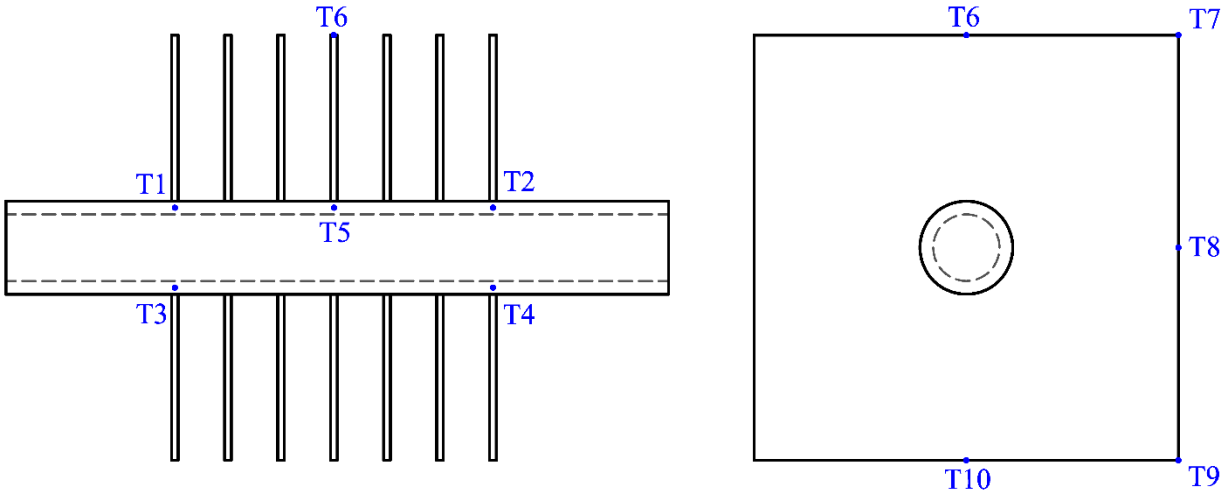

Fig. 5. Thermocouple number 1 to 10 configurations on each test case

As a result of the high thermal conductivity of aluminum, temperature differences are less than 10% for most cases. Therefore, we assumed that the average temperature of the thermocouple numbers 1 to 5 is the inner surface temperature (T_i) in Eq. (5), and the average temperature of thermocouple numbers 6 to 10 is the outer surface temperature of the fins (T_o) in Eq. (6). Based on these assumptions, Eq. (4) can be rewritten as follows:

$$Q_{rad} = \frac{(n-1)A_i \sigma\left(T_i^4 - T_a^4\right)}{\frac{1-\varepsilon_{al}}{\varepsilon_{al}} + \frac{1}{F_{i-a}}} + \left[n A_{o_f} \varepsilon_{al} \sigma\left(T_o^4 - T_a^4\right)\right]. \quad (7)$$

Table 3 lists the view factors for different surfaces of three finned tubes, shown in Fig. 6, and Table 4 shows the contribution of radiation heat transfer for each finned-tube experiment. Figure 7(a) illustrates radiation heat transfer rate delivered to the surroundings for various fin spacing. For the same input power, an increase in fin spacing results in a decrease in the radiation heat transfer rate from finned-tube surfaces because of a decrease in the heat transfer surface area. Figure 7(b) shows the fraction of heat transferred by radiation from total input power for various fin spacings.

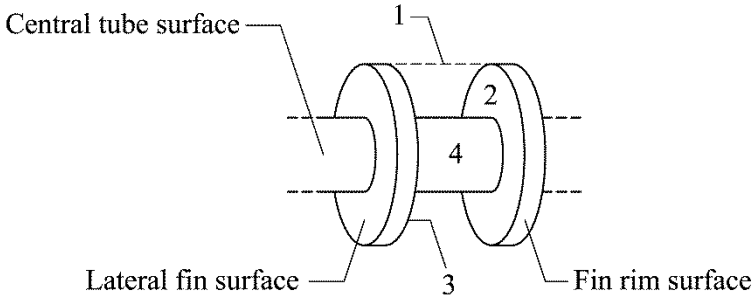

Fig. 6. Surfaces of a finned tube

Table 3. View factors between the spaces of two adjacent fins

Fin spacing (mm)	F_{1-1}	F_{1-2}	F_{1-4}	F_{2-3}	F_{2-4}	F_{1-i}	$F_{i-1} = F_{i-a}$
5	0.036	0.473	0.018	0.888	0.022	0.964	0.089
9	0.064	0.452	0.031	0.809	0.037	0.935	0.152
14	0.097	0.427	0.048	0.721	0.053	0.902	0.224

Table 4. Thermal radiation from three finned tubes.

Fin spacing, s (mm)	Test number	$Q_{Total} = EI\,(W)$	$q_{rad\_i}\,(W)$	$q_{rad\_o}\,(W)$	$q_{rad\_Total}\,(W)$	$\frac{q_{rad}}{Q_{Total}} \times 100$
5	1	8.7	0.924	0.066	0.990	11.4
	2	19.0	1.874	0.133	2.008	10.57
	3	33.6	3.088	0.217	3.305	9.84
	4	54.0	4.622	0.323	4.945	9.16
9	5	8.4	0.587	0.033	0.620	7.39
	6	19.0	1.267	0.070	1.338	7.04
	7	33.6	2.256	0.123	2.383	7.09
	8	55.8	3.435	0.187	3.622	6.49
14	9	8.4	0.501	0.024	0.526	6.26
	10	18.5	1.143	0.055	1.198	6.31
	11	34.3	2.098	0.099	2.198	6.41
	12	56.7	3.383	0.157	3.541	6.24

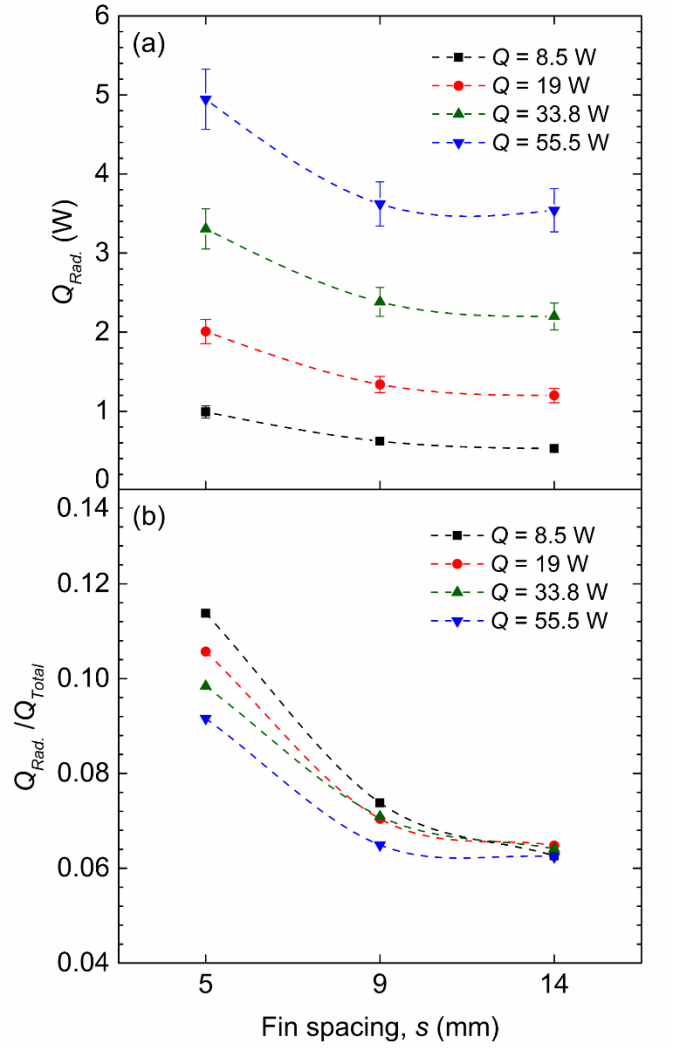

Fig. 7. (a) Variations in heat transfer radiation for various fin spacing and input power levels, and (b) the fraction of heat transfer caused by radiation from the total input power for various fin spacing and input power levels

3.3 Heat loss from end surfaces

To minimize heat loss from end surfaces, we use glass wool with a thermal conductivity of 0.04 $W.m^{-1}.K^{-1}$ for insulation. To calculate heat loss from the insulation surface at the steady-state condition, this study uses a contact thermometer Testo-925 with an accuracy of ±0.5°C to measure temperatures of various points on the insulation surface. Applying a method proposed by Jafarpur and Yovanovich [21, 22], we computed convection heat transfer coefficient for insulation and determined heat loss from end surfaces. The computed heat loss for various fin spacing is illustrated in Fig. 8, which shows as the power input increases, the heat loss from end

insulation surfaces increases, but the ratio of heat loss to the total heat input remains nearly constant. The end heat loss is less than 7% for all power input levels, which shows that end surfaces are appropriately insulated.

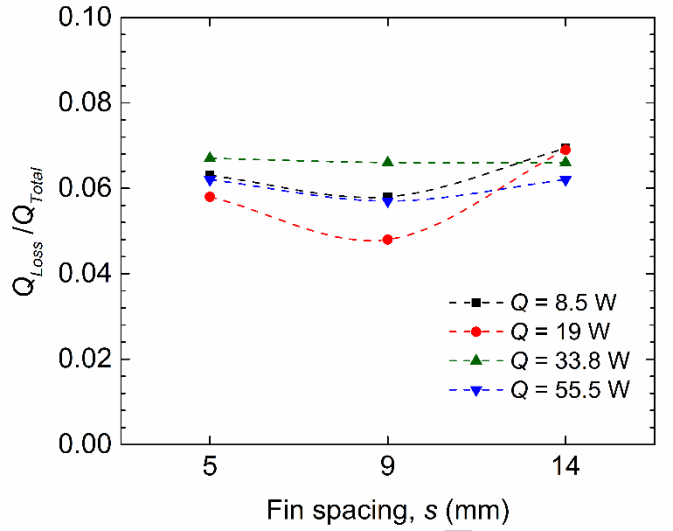

Fig. 8. Fraction of heat loss from total input power for various fin spacing and input power levels

3.4 Convection heat transfer rate

With radiation heat transfer rate and heat loss from the end surfaces, we computed the net rate of the convection heat transfer rate. Figure 9 illustrates the share of each mode of heat transfer from the total input power for various fin spacings. This figure shows that for all levels of input power, the share of radiation heat transfer is less than 10%, as is heat loss from the insulation surface. For all three fin spacings, the convection heat transfer part constitutes more than 80%.

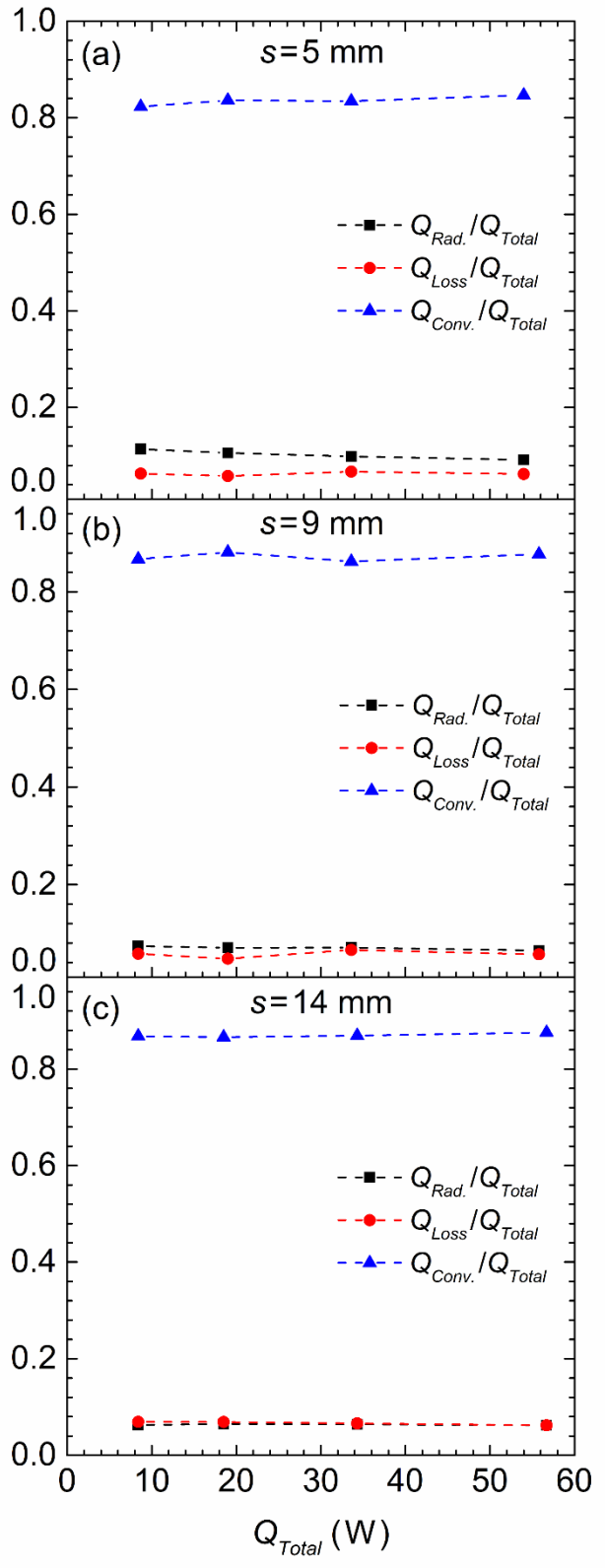

Fig. 9. Share of each mode of heat transfer from the total input power for various fin spacings

With convection heat transfer rate, one can find Nusselt number and fin effectiveness value using the following relations.

$$Ra_s^* = \frac{g\beta\Delta T s^3}{\alpha\nu}\frac{s}{L} \tag{8}$$

$$\bar{h} = \frac{Q_{conv}}{A_{Total}\,\Delta T} \tag{9}$$

$$\overline{Nu_s} = \frac{\bar{h}s}{k} \tag{10}$$

$$\varepsilon_f = \frac{q_f}{\bar{h}_b A_b \left(T_b - T_a\right)} \tag{11}$$

To ensure the validity of computed convection heat transfer, we compared the relations proposed by [3, 8] to our results. To compute the Rayleigh number in this comparison, the equivalent diameter $\left(D_e\right)$ is used for characteristic length and results are illustrated in Fig. 10. This figure shows that the Nusselt numbers from the experiments in this study follow the same trend as those predicted in [3, 8]. The differences in large Rayleigh number may result from approximation of squared fins with annular fins. Figures 11 and 12 present results of convection heat transfer rate and its related parameters.

Figure 11 shows convection heat transfer coefficient of the finned-tube geometry versus convection heat transfer rate. This figure shows that increasing the rate of convection heat transfer leads to an increase in the convection heat transfer coefficient. This figure also shows that as the fin spacing increases, the convection heat transfer coefficient increases. This augmentation is not uniform; that is, augmentation from 5 mm to 9 mm is greater than augmentation from 9 mm to 14 mm. Convection heat transfer is also related to the heat transfer area; hence, a product of the convection heat transfer coefficient and the total heat transfer area is shown in Fig. 12. The figure shows that when the fin spacing increases from 5 mm to 9 mm, product hA increases, and when it increases from 9 mm to 14 mm, the product decreases. These changes indicate that the best value of fin spacing is about 9 mm. These results are also observed in [9, 11] for annular fins. Figure 13 shows that an increase in the fin spacing leads to an increase in the heat transfer coefficient despite a decrease in the heat transfer surface area. Therefore, it

shows that increasing number of fins does not necessarily result in more heat transfer and that the fin spacing is optimal.

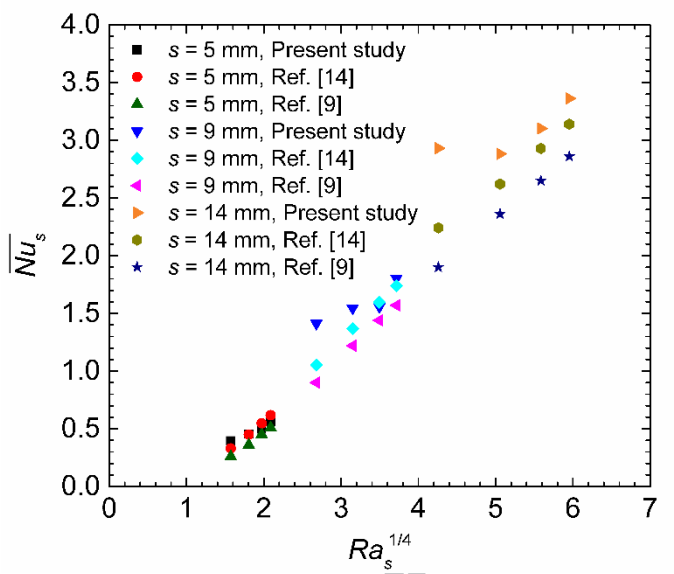

Fig. 10. Comparison of the average Nusselt number versus the Rayleigh number for various fin spacings

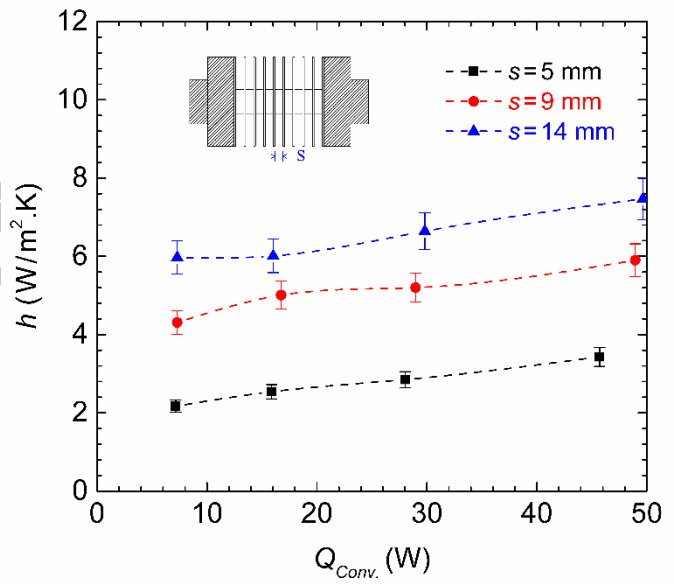

Fig. 11. Variation of convection heat transfer coefficient with convection heat transfer rate for different fin spacings

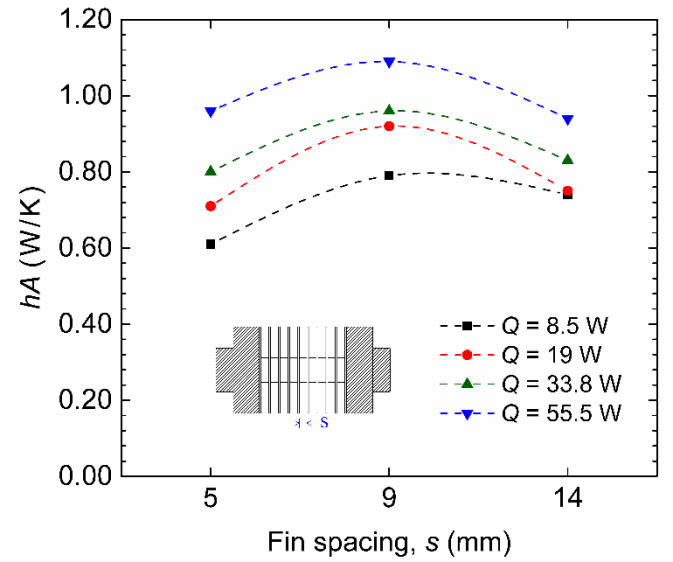

Fig. 12. Variation of multiple convection heat transfer coefficients and heat transfer surface area versus fin spacing

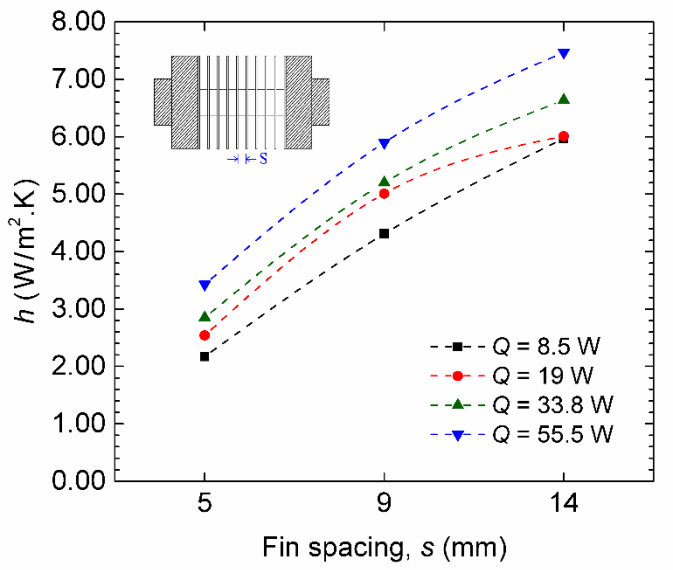

Fig. 13. Convection heat transfer coefficient with fin spacing for different input power

Difference between the average temperature of the finned-tube surface and the ambient temperature is a key parameter to find an appropriate fin for a specific application. Figure 14 illustrates variations in this parameter for various fin spacings and total input power levels. This figure shows that the minimum temperature difference occurs for the finned tube with a fin spacing of 9 mm. In addition, at higher levels of thermal input power, temperature differences

between three test cases are larger. This observation may result from an increase in the share of convection heat transfer, shown in Fig. 9; therefore, variations in the fin spacing affect resistance to the air flow between fins, and consequently temperature differences between the test case and the ambient environment. Figure 15 illustrates variations in the Nusselt number as a function of the Rayleigh number for fin spacings of 5, 9 and 14 mm. Here, the parameter $Ra_s^{*1/4}$ is used according to [8, 10, 11]. This figure shows that an increase in the Rayleigh number results in an increase in the average Nusselt number and the average convection heat transfer. In addition, the Rayleigh number approximately has a linear relationship with the Nusselt number.

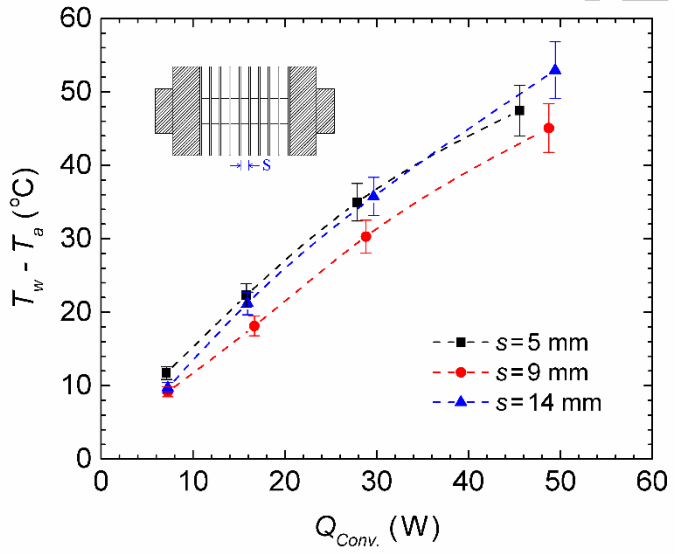

Fig. 14. Temperature difference between central tube surface and ambient environment for various fin spacing

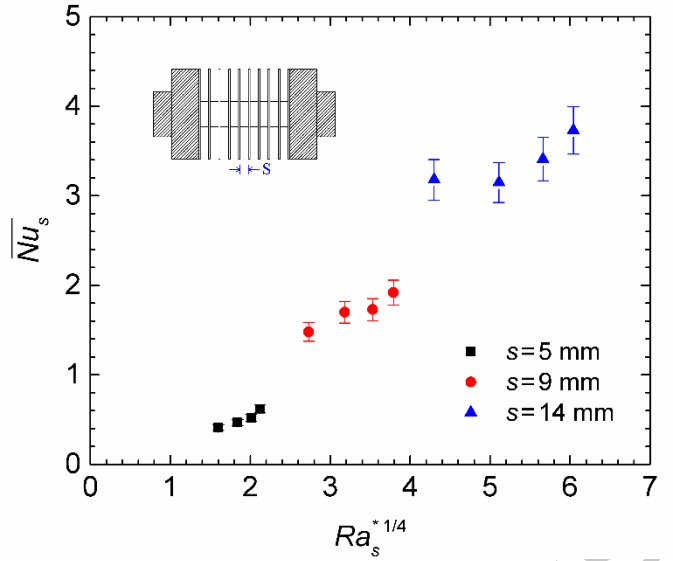

Fig. 15. Variations in average Nusselt number versus Rayleigh number for various fin spacings

To determine the performance of fins, we used the fin effectiveness parameter [19], which is the ratio of the heat transfer rate from an array of fins to the heat transfer rate from a bare cylinder of the same size without fins. In general, the main goal in designing of extended surfaces is to maximize the fin effectiveness, and using the finned surfaces with fin effectiveness values lower than two is not recommendable. Equation (11) determines the performance of fins, and Fig. 16 illustrates the fin effectiveness in the experiments for various fin spacings and input power levels. The results show that for all three fin spacings, the rate of heat transfer in comparison to a bare cylinder of the same size without fins significantly increases. In the experiments, the minimum and maximum values of the fin effectiveness are 12.8 and 17.8, respectively. Figure 16 shows that the fin effectiveness is maximum for a fin spacing of 9 mm and input power of 8.5 watts, and fin effectiveness reaches a desirable value of 17.8.

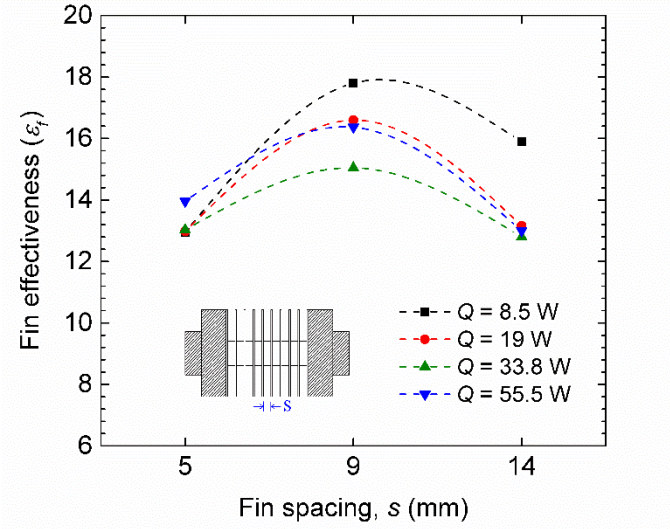

Fig. 16. Variations in fin effectiveness versus fin spacing for various input power levels

3.5 Correlation

Based on experimental results, we find a new correlation to predict Nusselt number of finned tubes with an array of square fins for natural convection and steady-state condition. Factors that affect convection heat transfer rate from array of square fins are ambient temperature (T_a), average temperature of fin surface (T_s), fin height (L), diameter of the inner tube (d), and fin spacing (s). The Nusselt number and the Rayleigh number are

$$\overline{Nu}_s = \frac{\bar{h}s}{k_a}, \tag{12}$$

$$Ra_s^* = \frac{g\beta(T_s - T_a)s^3}{\alpha\nu}\left(\frac{s}{L}\right), \tag{13}$$

where $\bar{h}$, k_a, g, β, α, and ν represent average convection heat transfer coefficient, thermal conductivity of air, acceleration of gravity, volumetric thermal expansion coefficient of air, thermal diffusivity, and the kinematic viscosity of air, respectively. The properties of air are determined at the film temperature,

$$T_f = \frac{T_s + T_a}{2}. \tag{14}$$

With a good approximation, the Nusselt number has a linear relationship with the Rayleigh number to the power of 0.25. Therefore, using experimental data and the least-squares method [23], we find a relationship between the Nusselt number $\left(Nu_s\right)$ and the Rayleigh number $\left(Ra_s^*\right)$ as follows:

$$Nu_s = 0.768 Ra_s^{*1/4} - 0.854 . \quad (15)$$

The correlation equation is valid for $6.5 \le Ra_s^{*1/4} \le 1335$ and an array of identical fins with the thickness of 0.002 m and the height of 0.1 m. The coefficient of determination $\left(r^2\right)$ is a statistical measure of how well the regression line approximates the real data points. The values of r^2 varies between 0 and 1, which $r^2 = 1$ indicates that the regression line perfectly fits the data points. For the derived correlation, the coefficient of determination is 0.96, which shows the regression line fits the results very well. Figure 17 illustrates the Nusselt numbers from experimental measurements and the predicted values from Eq. (15) versus the Rayleigh number, which are in a good agreement. Only in one experiment with a relatively large Rayleigh number, a higher deviation is observed between experimental measurements and predicted values from the correlation. The experimental measurements of the Nusselt number versus the calculated ones from the correlation are plotted in Fig. 18. This figure shows that the developed correlation precisely predicts the Nusselt number for finned tubes with square fins.

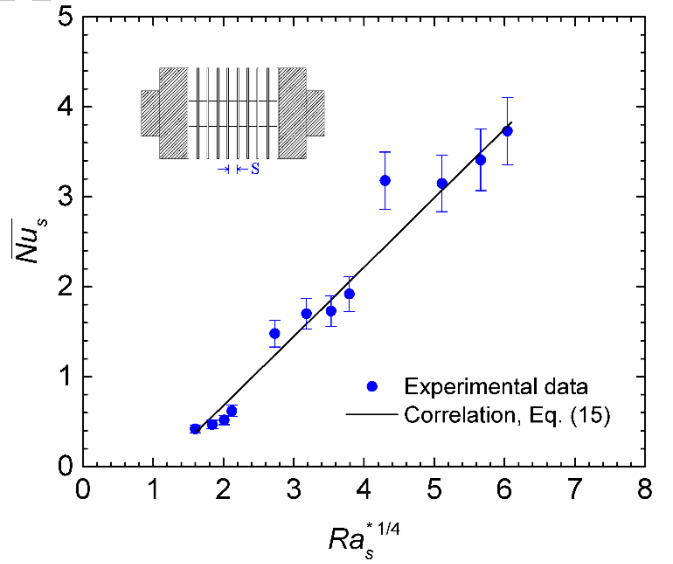

Fig. 17. Comparison of experimental measurements and correlation equation predictions

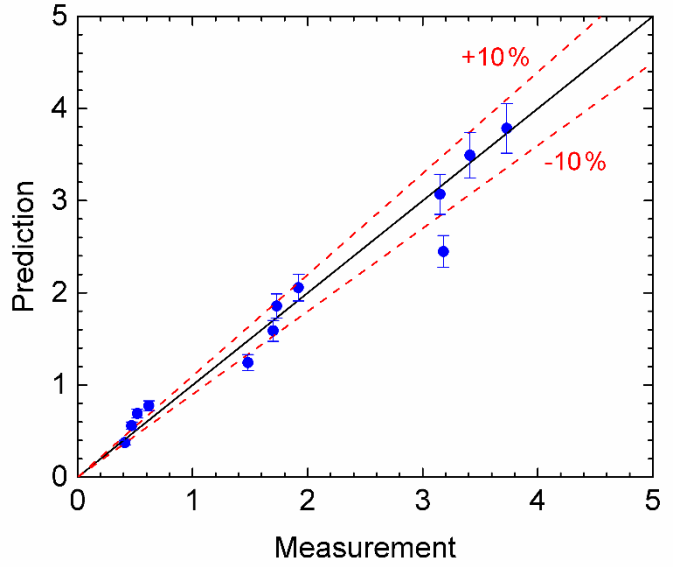

Fig. 18. Comparison of experimental measurements and predicted values by Eq. (15)

4. Uncertainty analysis

The uncertainty analysis (i.e., error propagation analysis) addresses how the error sources lead to the uncertainty of a derived quantity. Therefore, the uncertainty analysis is necessary in any experimental study. Accuracy and uncertainty indeed have an inverse relationship with each other, in the other words, high accuracy of measurement decreases the uncertainty and vice versa. In the experiments, we used several instruments with error values listed in

Table 5. In addition, Table 6 summaries the uncertainty of the Eq. (15) and other used parameters, which are calculated according to [17, 24].

Table 5. Measurement accuracy of the parameters.

Measurement	Accuracy
Test case temperature	±0.50 °C
Ambient air temperature	±0.40 °C
Test room wall temperature	±0.30 °C
Testo 925 thermometer	±0.50 °C
Fin height and spacing	±0.02 mm

Table 6. Uncertainty of the calculated parameters and the correlation prediction.

Parameter	Uncertainty (%)
Temperature difference between fin base and ambient air	7.3
Total heat rate	3.5
Radiation heat transfer	7.7
Convection heat transfer	4.6
Convection heat transfer coefficient, $\bar{h}$	7.1
Nusselt number, Eq. (10)	7.1
Nusselt number, Eq. (15)	9.7

5. Conclusion

In this research, we experimentally studied natural convection heat transfer of finned-tube exchangers with an array of square fins. In the experiments, temperature and humidity are automatically controlled with heating, cooling, humidifying, and dehumidifying equipment. We changed surface temperature of the center tube by varying input power of the heating element from 8.4 to 56.7 watts. We conducted multiple experiments for each exchanger and measured its temperature under steady-state condition with ten T-type thermocouples. We also calculate the average natural convection heat transfer coefficient. The results show that maximum fraction of input power radiated to the ambient environment is less than 11.6%. However, the share of natural convection from input power is about 80%. In addition, an increase in convection heat transfer rate or the fin spacing causes an increase in the average convection heat transfer coefficient. Moreover, in the experiments, fin effectiveness is in a desired range of 12.8-17.8, and optimum fin spacing is 9 mm. Finally, this study established an empirical relationship in an equation for predicting average Nusselt number when Rayleigh number is between 6.5 and 1,335, based on the fin spacing.

Acknowledgment

This study was partially supported by Iran's National Elites Foundation and the authors acknowledge the support.

References

[1] W. Elenbaas, "Heat dissipation of parallel plates by free convection," *Physica*, vol. 9, pp. 1-28, 1942.

[2] E. Sparrow and P. Bahrami, "Experiments on natural convection heat transfer on the fins of a finned horizontal tube," *International Journal of Heat and Mass Transfer,* vol. 23, pp. 1555-1560, 1980.

[3] J. Edwards and J. Chaddock, "An experimental investigation of the radiation and free convection heat transfer from a cylindrical disk extended surface," *Trans. Am. Soc. Heat. Refrig. Air-Cond. Eng,* vol. 69, pp. 313-322, 1963.

[4] J. Knudsen and R. Pan, "Natural convection heat transfer from transverse finned tubes," 59, Chem. Eng. Progr, 1963.

[5] C. Jones, "Optimum Spacing of Circular Fins on Horizontal Tubes for Natural Convection Heat Transfer," in *ASHRAE JOURNAL*, 1969, pp. 72-&.

[6] N. Kayansayan and R. Karabacak, "Natural convection heat transfer coefficients for a horizontal cylinder with vertically attached circular fins," *Heat Recovery Systems and CHP,* vol. 12, pp. 457-468, 1992.

[7] E. Hahne and D. Zhu, "Natural convection heat transfer on finned tubes in air," *International journal of heat and mass transfer,* vol. 37, pp. 59-63, 1994.

[8] C. Wang, M. Yovanovich, and J. Culham, "General model for natural convection: application to annular-fin heat sinks," *ASME-PUBLICATIONS-HTD,* vol. 343, pp. 119-128, 1997.

[9] Ş. Yildiz and H. Yüncü, "An experimental investigation on performance of annular fins on a horizontal cylinder in free convection heat transfer," *Heat and mass transfer,* vol. 40, pp. 239-251, 2004.

[10] H.-T. Chen and J.-C. Chou, "Investigation of natural-convection heat transfer coefficient on a vertical square fin of finned-tube heat exchangers," *International journal of heat and mass transfer,* vol. 49, pp. 3034-3044, 2006.

[11] H.-T. Chen and W.-L. Hsu, "Estimation of heat transfer coefficient on the fin of annular-finned tube heat exchangers in natural convection for various fin spacings," *International journal of heat and mass transfer,* vol. 50, pp. 1750-1761, 2007.

[12] B. H. An, H. J. Kim, and D.-K. Kim, "Nusselt number correlation for natural convection from vertical cylinders with vertically oriented plate fins," *Experimental Thermal and Fluid Science,* vol. 41, pp. 59-66, 2012.

[13] K. T. Park, H. J. Kim, and D.-K. Kim, "Experimental study of natural convection from vertical cylinders with branched fins," *Experimental Thermal and Fluid Science,* vol. 54, pp. 29-37, 2014.

[14] M. Lee, H. J. Kim, and D.-K. Kim, "Nusselt number correlation for natural convection from vertical cylinders with triangular fins," *Applied Thermal Engineering,* vol. 93, pp. 1238-1247, 2016.

[15] M. Torabi, A. Keyhani, and G. P. Peterson, "A comprehensive investigation of natural convection inside a partially differentially heated cavity with a thin fin using two-set lattice Boltzmann distribution functions," *International Journal of Heat and Mass Transfer,* vol. 115, pp. 264-277, 2017/12/01/ 2017.

[16] M. Amini, A. R. Pishevar, and M. Yaghoubi, *Experimental study of frost formation on a fin-and-tube heat exchanger by natural convection* vol. 46, 2014.

[17] K. Hirbodi and M. Yaghoubi, "Experimental investigation of natural dehumidification over an annular finned-tube," *Experimental Thermal and Fluid Science,* vol. 57, pp. 128-144, 2014.

[18] A. R. Tahavvor and M. Yaghoubi, "Experimental and numerical study of frost formation by natural convection over a cold horizontal circular cylinder," *International Journal of Refrigeration,* vol. 33, pp. 1444-1458, 2010.

[19] T. L. Bergman, F. P. Incropera, and A. S. Lavine, *Fundamentals of heat and mass transfer*: John Wiley & Sons, 2011.

[20] C. Tso, Y. Cheng, and A. Lai, "An improved model for predicting performance of finned tube heat exchanger under frosting condition, with frost thickness variation along fin," *Applied Thermal Engineering*, vol. 26, pp. 111-120, 2006.

[21] K. Jafarpur and M. Yovanovichy, "Natural Convection from Horizontal Isothermal Elliptic Disks: Models and Experiments," in *Proc. 35th Aerospace Sciences Meeting & Exhibit, AIAA, Reno, NV*, 1997.

[22] M. Yovanovich and K. Jafarpur, "Models of Laminar Natural Convection From Vertical and Horizontal Isothermal Cuboids for All Prandtl Numbers and All Rayleigh Numbers Below 10^ 1^ 1," *ASME-PUBLICATIONS-HTD*, vol. 264, pp. 111-111, 1993.

[23] R. E. Walpole, R. H. Myers, S. L. Myers, and K. Ye, *Probability and statistics for engineers and scientists* vol. 5: Macmillan New York, 1993.

[24] L. Kirkup and R. B. Frenkel, *An Introduction to Uncertainty in Measurement: Using the GUM (Guide to the Expression of Uncertainty in Measurement)*: Cambridge University Press, 2006.

1. Natural convection heat transfer of three square finned-tube exchangers is investigated experimentally.
2. Average natural heat transfer coefficient increases to a certain value by increasing the fin spacing.
3. Fin effectiveness has a maximum value for a certain fin spacing of s=9 mm.
4. A new correlation is developed for Nu_s as a function of Rayleigh number :

$$Nu_s = 0.768 Ra_s^{1/4} - 0.854$$

for $6.5 < Ra_s < 1335$